EUROPEAN ORGANISATION FOR NUCLEAR RESEARCH

CERN-EP/90-81
June 11 1990

# Analysis of $Z^0$ Couplings to Charged Leptons


The OPAL Collaboration

**Abstract**

The couplings of the $Z^0$ to charged leptons are studied using measurements of the lepton pair cross sections and forward-backward asymmetries at centre of mass energies near to the mass of the $Z^0$. The data are consistent with lepton universality. Using a parametrisation of the lepton pair differential cross section which assumes that the $Z^0$ has only vector and axial vector couplings to leptons, the charged leptonic partial decay width of the $Z^0$ is determined to be $\Gamma_{l^+l^-} = 83.1 \pm 1.9$ MeV and the square of the product of the effective axial vector and vector coupling constants of the $Z^0$ to charged leptons to be $\hat{a}_l^2 \hat{v}_l^2 = 0.0039 \pm 0.0083$, in agreement with the Standard Model. A parametrisation in the form of the improved Born approximation gives effective leptonic axial vector and vector coupling constants $\hat{a}_l^2 = 0.998 \pm 0.024$ and $\hat{v}_l^2 = 0.0044 \pm 0.0083$. In the framework of the Standard Model, the values of the parameters $\rho_Z$ and $\sin^2\overline{\theta}_W$ are found to be $0.998 \pm 0.024$ and $0.233^{+0.045}_{-0.012}$ respectively. Using the relationship in the minimal Standard Model between $\rho_Z$ and $\sin^2\overline{\theta}_W$, the result $\sin^2\overline{\theta}_W^{SM} = 0.233^{+0.007}_{-0.006} \pm 0.002$ is obtained, where the first error is experimental and the second is theoretical. Our previously published measurement of the ratio of the hadronic to the leptonic partial width of the $Z^0$ is updated: $R_Z = 21.72^{+0.71}_{-0.65}$.

(submitted to Physics Letters B)

# The OPAL Collaboration


M.Z. Akrawy[11], G. Alexander[21], J. Allison[14], P.P. Allport[5], K.J. Anderson[8], J.C. Armitage[6], G.T.J. Arnison[18], P. Ashton[14], G. Azuelos[16,f], J.T.M. Baines[14], A.H. Ball[15], J. Banks[14], G.J. Barker[11], R.J. Barlow[14], J.R. Batley[5], J. Becker[9], T. Behnke[7], K.W. Bell[18], G. Bella[21], S. Bethke[10], O. Biebel[3], U. Binder[9], I.J. Bloodworth[1], P. Bock[10], H. Breuker[7], R.M. Brown[18], R. Brun[7], A. Buijs[7], H.J. Burckhart[7], P. Capiluppi[2], R.K. Carnegie[6], A.A. Carter[11], J.R. Carter[5], C.Y. Chang[15], D.G. Charlton[7], J.T.M. Chrin[14], P.E.L. Clarke[23], I. Cohen[21], W.J. Collins[5], J.E. Conboy[13], M. Couch[1], M. Coupland[12], M. Cuffiani[2], S. Dado[20], G.M. Dallavalle[2], P. Debu[19], M.M. Deninno[2], A. Dieckmann[10], M. Dittmar[4], M.S. Dixit[17], E. Duchovni[24], I.P. Duerdoth[7,d], D. Dumas[6], H. El Mamouni[16], P.A. Elcombe[5], P.G. Estabrooks[6], E. Etzion[21], F. Fabbri[2], P. Farthouat[19], H.M. Fischer[3], D.G. Fong[15], M.T. French[18], C. Fukunaga[22], A. Gaidot[19], O. Ganel[24], J.W. Gary[10], J. Gascon[16], N.I. Geddes[18], C.N.P. Gee[18], C. Geich-Gimbel[3], S.W. Gensler[8], F.X. Gentit[19], G. Giacomelli[2], V. Gibson[5], W.R. Gibson[11], J.D. Gillies[18], J. Goldberg[20], M.J. Goodrick[5], W. Gorn[4], D. Granite[20], E. Gross[24], J. Grunhaus[21], H. Hagedorn[9], J. Hagemann[7], M. Hansroul[7], C.K. Hargrove[17], J. Hart[5], P.M. Hattersley[1], M. Hauschild[7], C.M. Hawkes[7], E. Heflin[4], R.J. Hemingway[6], R.D. Heuer[7], J.C. Hill[5], S.J. Hillier[1], C. Ho[4], J.D. Hobbs[8], P.R. Hobson[23], D. Hochman[24], B. Holl[7], R.J. Homer[1], S.R. Hou[15], C.P. Howarth[13], R. Humbert[9], R.E. Hughes-Jones[14], P. Igo-Kemenes[10], H. Ihssen[10], D.C. Imrie[23], A. Jawahery[15], P.W. Jeffreys[18], H. Jeremie[16], M. Jimack[7], M. Jobes[1], R.W.L. Jones[11], P. Jovanovic[1], D. Karlen[6], K. Kawagoe[22], T. Kawamoto[22], R.G. Kellogg[15], B.W. Kennedy[13], C. Kleinwort[7], D.E. Klem[17], G. Knop[3], T. Kobayashi[22], T.P. Kokott[3], L. Köpke[7], R. Kowalewski[6], H. Kreutzmann[3], J. von Krogh[10], J. Kroll[8], M. Kuwano[22], P. Kyberd[11], G.D. Lafferty[14], F. Lamarche[16], W.J. Larson[4], J.G. Layter[4], P. Le Du[19], P. Leblanc[16], A.M. Lee[15], M.H. Lehto[13], D. Lellouch[7], P. Lennert[10], L. Lessard[16], L. Levinson[24], S.L. Lloyd[11], F.K. Loebinger[14], J.M. Lorah[15], B. Lorazo[16], M.J. Losty[17], J. Ludwig[9], N. Lupu[20], J. Ma[4,b], A.A. Macbeth[14], M. Mannelli[7], S. Marcellini[2], G. Maringer[3], A.J. Martin[11], J.P. Martin[16], T. Mashimo[22], P. Mättig[7], U. Maur[3], T.J. McMahon[1], J.R. McNutt[23], A.C. McPherson[6,c], F. Meijers[7], D. Menszner[10], F.S. Merritt[8], H. Mes[17], A. Michelini[7], R.P. Middleton[18], G. Mikenberg[24], D.J. Miller[13], C. Milstene[21], M. Minowa[22], W. Mohr[9], A. Montanari[2], T. Mori[22], M.W. Moss[14], P.G. Murphy[14], W.J. Murray[5], B. Nellen[3], H.H. Nguyen[8], M. Nozaki[22], A.J.P. O'Dowd[14], S.W. O'Neale[7,e], B.P. O'Neill[4], F.G. Oakham[17], F. Odorici[2], M. Ogg[6], H. Oh[4], M.J. Oreglia[8], S. Orito[22], J.P. Pansart[19], G.N. Patrick[18], S.J. Pawley[14], P. Pfister[9], J.E. Pilcher[8], J.L. Pinfold[24], D.E. Plane[7], B. Poli[2], A. Pouladdej[6], T.W. Pritchard[11], G. Quast[7], J. Raab[7], M.W. Redmond[8], D.L. Rees[1], M. Regimbald[16], K. Riles[4], C.M. Roach[5], S.A. Robins[11], A. Rollnik[3], J.M. Roney[8], S. Rossberg[9], A.M. Rossi[2,a], P. Routenburg[6], K. Runge[9], O. Runolfsson[7], S. Sanghera[6], R.A. Sansum[18], M. Sasaki[22], B.J. Saunders[18], A.D. Schaile[9], O. Schaile[9], W. Schappert[6], P. Scharff-Hansen[7], H. von der Schmitt[10], S. Schreiber[3], J. Schwarz[9], A. Shapira[24], B.C. Shen[4], P. Sherwood[13], A. Simon[3], P. Singh[11], G.P. Siroli[2], A. Skuja[15], A.M. Smith[7], T.J. Smith[1], G.A. Snow[15], E.J. Spreadbury[13,†], R.W. Springer[15], M. Sproston[18], K. Stephens[14], H.E. Stier[9], R. Ströhmer[10], D. Strom[8], H. Takeda[22], T. Takeshita[22], T. Tsukamoto[22], M.F. Turner[5], G. Tysarczyk-Niemeyer[10], D. Van den plas[16], G.J. VanDalen[4], G. Vasseur[19], C.J. Virtue[17], A. Wagner[10], C. Wahl[9], C.P. Ward[5], D.R. Ward[5], J. Waterhouse[6], P.M. Watkins[1], A.T. Watson[1], N.K. Watson[1], M. Weber[10], S. Weisz[7], P.S. Wells[7], N. Wermes[10], M. Weymann[7], G.W. Wilson[19], J.A. Wilson[1], I. Wingerter[7], V-H. Winterer[9], N.C. Wood[13], S. Wotton[7], B. Wuensch[3], T.R. Wyatt[14], R. Yaari[24], Y. Yang[4,b], G. Yekutieli[24], T. Yoshida[22], W. Zeuner[7], G.T. Zorn[15]

[1]School of Physics and Space Research, University of Birmingham, Birmingham, B15 2TT, UK
[2]Dipartimento di Fisica dell' Università di Bologna and INFN, Bologna, 40126, Italy
[3]Physikalisches Institut, Universität Bonn, D-5300 Bonn 1, FRG
[4]Department of Physics, University of California, Riverside, CA 92521 USA
[5]Cavendish Laboratory, Cambridge, CB3 0HE, UK
[6]Carleton University, Dept of Physics, Colonel By Drive, Ottawa, Ontario K1S 5B6, Canada
[7]CERN, European Organisation for Particle Physics, 1211 Geneva 23, Switzerland
[8]Enrico Fermi Institute and Department of Physics, University of Chicago, Chicago Illinois 60637, USA
[9]Fakultät für Physik, Albert Ludwigs Universität, D-7800 Freiburg, FRG
[10]Physikalisches Institut, Universität Heidelberg, D-6900 Heidelberg, FRG
[11]Queen Mary and Westfield College, University of London, London, E1 4NS, UK
[12]Birkbeck College, London, WC1E 7HV, UK
[13]University College London, London, WC1E 6BT, UK
[14]Department of Physics, Schuster Laboratory, The University, Manchester, M13 9PL, UK
[15]Department of Physics and Astronomy, University of Maryland, College Park, Maryland 20742, USA
[16]Laboratoire de Physique Nucléaire, Université de Montréal, Montréal, Quebec, H3C 3J7, Canada
[17]National Research Council of Canada, Herzberg Institute of Astrophysics, Ottawa,
Ontario K1A 0R6, Canada
[18]Rutherford Appleton Laboratory, Chilton, Didcot, Oxfordshire, OX11 0QX, UK
[19]DPhPE, CEN Saclay, F-91191 Gif-sur-Yvette, France
[20]Department of Physics, Technion-Israel Institute of Technology, Haifa 32000, Israel
[21]Department of Physics and Astronomy, Tel Aviv University, Tel Aviv 69978, Israel
[22]International Centre for Elementary Particle Physics and Dept of Physics, University of Tokyo,
Tokyo 113, and Kobe University, Kobe 657, Japan
[23]Brunel University, Uxbridge, Middlesex, UB8 3PH UK
[24]Nuclear Physics Department, Weizmann Institute of Science, Rehovot, 76100, Israel

[a]Present address: Dipartimento di Fisica, Università della Calabria, 87036 Rende, Italy
[b]On leave from Harbin Institute of Technology, Harbin, China
[c]Now at Applied Silicon Inc
[d]On leave from Manchester University
[e]On leave from Birmingham University
[f]and TRIUMF, Vancouver, Canada
[†]deceased 6 February 1990

# 1 Introduction

The successful start of operations at LEP makes possible precision tests of the unified gauge theory of the electroweak interaction directly at the energy scale of the unification. In a recent publication [1] we used the entire data sample collected in 1989 with the OPAL detector to measure the mass of the $Z^0$ boson, its total decay width and peak cross section, and its partial decay widths into hadrons, charged leptons and invisible final states.

In this paper, an extended analysis of the charged leptonic final states is presented, based on 606 $e^+e^- \to e^+e^-$, 890 $e^+e^- \to \mu^+\mu^-$ and 871 $e^+e^- \to \tau^+\tau^-$ events, corresponding to an integrated luminosity of approximately 1 $pb^{-1}$. The cross sections and the forward-backward charge asymmetries were measured at several centre of mass energies around the $Z^0$ mass. For $\mu^+\mu^-$ and $\tau^+\tau^-$ events the geometrical acceptance has been extended, and for $\tau^+\tau^-$ events the selection efficiency has been increased, compared to the earlier analysis. Fits were performed to these data to determine the couplings of the $Z^0$ to charged leptons.

# 2 The OPAL detector

The data presented here were recorded with the OPAL detector [2] at the CERN $e^+e^-$ collider LEP during its 1989 operation. The tracking of charged particles was performed with a jet chamber, a large volume drift chamber divided into 24 azimuthal sectors with 159 layers of wires, together with a vertex detector and a z-chamber. These are positioned inside a solenoidal coil, which is surrounded by a time-of-flight counter array, a lead glass electromagnetic calorimeter with a presampler, an instrumented magnet return yoke serving as a hadron calorimeter and four layers of outer muon chambers. Forward detectors serve as a luminosity monitor. The momentum resolution is $\Delta p/p = 10\%$, for $p \approx 45$ GeV/c, and the electromagnetic energy resolution is $\Delta E/E = 3\%$, for $E \approx 45$ GeV.

Details of many of these detector components have been given in previous publications [3,4]. In addition, in this analysis, the endcap muon detection system is used. This consists of four layers of limited streamer tubes, grouped into two pairs separated by 70 cm. Each pair consists of one layer of horizontal and one layer of vertical tubes. Each layer of tubes has two sets of analog cathode readout strips, one parallel to the tubes and one perpendicular, allowing measurement of both x and y coordinates. The geometrical acceptance of the chambers is greater than 80% in the angular range $0.7 < |\cos\theta| < 0.86$, with the loss of acceptance being due to the cable paths for the central detectors.

A detailed description of the luminosity measurements is given in reference [1]. The systematic normalisation error was 2.2% and the point-to-point systematic error was 1.0%. The centre of mass energy, $\sqrt{s}$, is calculated from the beam energies measured by the SL Division (formerly LEP Division). The overall fractional scale uncertainty is $3 \times 10^{-4}$ (about 30 MeV) and the fractional point-to-point error is $1 \times 10^{-4}$.

For Monte Carlo studies the OPAL detector was simulated using a program [5] that includes the detector geometry and material as well as effects of detector resolutions and efficiencies.

# 3 The Leptonic Decays

The cross sections and the forward-backward charge asymmetries are obtained for each charged leptonic final state. The criteria used to select $e^+e^- \to e^+e^-$ and $e^+e^- \to \mu^+\mu^-$ events were similar to the ones described in detail in references [1,4]. In the present analysis, however, new selection cuts have been used for the $e^+e^- \to \tau^+\tau^-$ channel, giving a higher efficiency, and the angular region has been extended to $|\cos\theta| < 0.85$ for $\tau^+\tau^-$ and $|\cos\theta| < 0.82$ for $\mu^+\mu^-$. For each channel, the cross section is determined from a subset of the total data sample for which a reliable luminosity measurement could be made.

## 3.1 $e^+e^-$ channel

The first stage in the selection of $e^+e^-$ events required at least two lead glass clusters in the angular region $|\cos\theta| < 0.80$, each with at least 50% of the beam energy. The total reconstructed electromagnetic energy had to be greater than 85% of the centre of mass energy. To eliminate remaining background from multihadronic decays of the $Z^0$, the number of lead glass clusters was required to be less than 9 and the summed number of charged tracks and lead glass clusters less than 21. The background from $e^+e^- \to \gamma\gamma$ events was eliminated by requiring that each of the two highest energy clusters was associated with a charged track.

As described in Section 5.1, a program based on an analytic formula for the differential cross section of $e^+e^- \to e^+e^-(\gamma)$ was used to treat the photonic radiative corrections for the $e^+e^- \to e^+e^-$ data. This formula requires that, for $e^+e^-\gamma$ events, kinematic cuts be specified on the photon energy ($k$) and the opening angle ($\delta$) between the hard photon and a final-state lepton. For events with a detected hard photon these cuts can be applied directly to the data. We required $k < 0.083\,E_{\rm beam}$ or $\delta < 5°$, where $E_{\rm beam}$ is the beam energy. To reject events with an undetected hard photon emitted along the beam direction ($|\cos\theta| > 0.98$), the acollinearity angle between the two highest energy clusters was required to be less than 5°. This cut does not precisely correspond to the kinematic region defined by the cuts on $k$ and $\delta$. A correction has therefore to be applied in order to allow the measured cross section and asymmetry to be compared with the theory. The correction was obtained by using the BABAMC Monte Carlo [6]. The size of the correction to the cross section was -0.3% around the $Z^0$ peak and -5% at 95 GeV.

In order to minimise the contributions to the $e^+e^-$ cross section coming from $t$-channel exchange diagrams, a cut of $\cos\theta_{e^-} < 0.40$ was applied, where $\theta_{e^-}$ is the angle between the final state $e^-$ and the initial state $e^-$. The final $e^+e^- \to e^+e^-$ analysis was restricted to the limited angular region $-0.70 < \cos\theta_{e^-} < 0.40$.

A Monte Carlo calculation using the BABAMC generator has been made to determine the efficiency of these cuts. Within the angular acceptance given above, the efficiency is $99.1 \pm 0.7\%$. The trigger efficiency was checked by comparing a number of redundant triggers and found to be $> 99.9\%$. The background contamination has also been determined by a Monte Carlo calculation. The contribution from $\tau^+\tau^-$ pair production is calculated to be $0.1 \pm 0.1\%$, using the KORALZ generator [7]. This program generates $e^+e^- \to \mu^+\mu^-$ and $e^+e^- \to \tau^+\tau^-$ according to the Standard Model, including the effects from initial and final state radiation. The backgrounds from multihadronic events and the process $e^+e^- \to e^+e^-e^+e^-$ are estimated to be less than 0.1%.

The effects on the cross section and asymmetry of the finite angular resolution and possible systematic errors in the angular measurement were studied using the Monte Carlo simulation. The effect on

the cross section is negligible and the systematic error on the asymmetry is estimated to be less than 0.003. The signs of the charges of the tracks were determined from their curvature in the magnetic field. Events in which both tracks were assigned the same sign were not used for the asymmetry measurement. The probability for double assignment of the wrong charge in an event, which would affect the forward-backward asymmetry, is less than 0.2% and independent of $\cos\theta$ based on the observed number of events in which both tracks had been assigned the same charge.

### 3.2 $\mu^+\mu^-$ channel

Candidate $\mu^+\mu^-$ events were selected from a sample of events flagged by an online filter [4], and which in addition contained less than 13 lead glass clusters with energy above 250 MeV and less than 11 charged tracks with $p_T > 100$ MeV, where $p_T$ is the momentum of the track in the plane perpendicular to the electron-positron beam direction.

Events were classified as $\mu^+\mu^-$ candidates if they contained at least two charged tracks identified as muons. Both tracks had to satisfy the requirements: $p > 6$ GeV, $|\cos\theta| < 0.82$, and $d_0 < 1$ cm, where $d_0$ is the distance of closest approach of the track to the beam axis. The acollinearity angle between the two tracks ($\theta_{acol}$) had to be less than 15°. A track was classified as a muon if it satisfied any one of the following four criteria: i) there were at least two hits in the barrel muon chambers associated with the track within $\Delta\phi = 70$ mrad; ii) within $\Delta\phi = 70$ mrad there was a track segment in the endcap muon chambers; iii) within $\Delta\phi = 70$ mrad there was a track segment in the barrel hadron calorimeter; with hits in at least five of the nine layers; iv) the momentum, $p$, was larger than 15 GeV and the sum of the energies in the barrel lead glass of all clusters within $\Delta\phi = 200$ mrad was less than 3 GeV. The cuts on $\theta_{acol}$ and $p$ reduced the background from $e^+e^- \to e^+e^-\mu^+\mu^-$, the cut on $p$ suppressed the background from $e^+e^- \to \tau^+\tau^-$, and the cut on $d_0$ suppressed the background from cosmic rays. Information from the TOF counters was used to remove the remaining background from cosmic rays by rejecting events that were not in time with the beam crossing and by distinguishing between a single particle traversing the detector and a pair of particles produced at the interaction point. Events were required to contain at least one TOF counter that measured a time within 10 ns of that expected for a particle coming from the interaction point. In addition, we considered the difference, $\Delta t$, between the times measured by pairs of TOF counters separated in azimuth by more than 165°; events in which $\Delta t > 10$ ns for all such pairs were rejected as cosmic rays.

Triggers for $\mu^+\mu^-$ events were provided by the central detector, the TOF counters, and the muon chambers. The resulting high degree of redundancy enabled the efficiencies of the individual components to be measured using the $\mu^+\mu^-$ events themselves. In this way the efficiency of the combined trigger was found to be $99.2 \pm 0.5\%$. The efficiency of the online filter was found in a similar study to be $99.5 \pm 0.5\%$.

The acceptance of the requirement that two tracks be within $|\cos\theta| < 0.82$ was evaluated using $\mu^+\mu^-$ events generated with the KORALZ Monte Carlo program [7] and then passed through the detector simulation. It is $75.0 \pm 1.0\%$ at $\sqrt{s} = M_Z$ and varies by 1% over the range of the energy scan. Using the same program, a background of $3.7 \pm 0.9\%$ from $e^+e^- \to \tau^+\tau^-$ was calculated. From a Monte Carlo simulation [8] of $e^+e^- \to e^+e^-\mu^+\mu^-$ a background of $0.1 \pm 0.1\%$ was found.

Systematic checks of the analysis revealed a number of imperfections in the simulation of the detector by the Monte Carlo program. An additional efficiency factor of $99 \pm 1\%$ was included to account for this fact. Combining the efficiency, acceptance and background gives an overall correction factor of $1.31 \pm 0.03$ for the number of $\mu^+\mu^-$ events. Events in which both muons were assigned the

same charge were not used for the asymmetry measurement. From the number of these events, the probability for double assignment of the wrong charge was found to be less than 0.2%.

### 3.3 $\tau^+\tau^-$ channel

The $\tau^+\tau^-$ events were selected by the following criteria. The number of charged tracks had to be between 2 and 6, and the number of lead glass clusters less than 11, where the cluster threshold energy was chosen to be 100 and 200 MeV for the barrel and endcap parts respectively. This cut was effective in eliminating the background from multihadronic events. In order to reject background from $e^+e^-$ and $\mu^+\mu^-$ events and from two-photon processes, the total observed calorimeter energy in the lead glass calorimeter was required to be between 3% and 80% of the centre of mass energy, and the total visible energy to be between 18% and 120%, where the total visible energy was defined as the scalar sum of the electromagnetic energy and the momenta of charged tracks. These differ from the cuts used in our previous publications [1,4] and lead to a higher $\tau^+\tau^-$ selection efficiency. The $\mu^+\mu^-$ events identified by the criteria described in subsection 3.2 were removed. In order to reject cosmic rays, the vertex position along the beam direction was required to be less than 30 cm from the beam crossing point, and at least one track had to have a distance of closest approach to the beam axis of less than 0.5 cm. A cut was made on the direction of the sum of the energy vectors measured in the lead glass with respect to the beam axis of $|\cos\theta| < 0.95$. This cut removed backgrounds from two-photon processes and beam gas interactions.

The identification of $\tau$ candidates was performed by combining the observed particles, both charged tracks and lead glass clusters, in the following way. First the highest energy particle in the event was selected and a cone with a half opening angle of 35 degrees was defined around it. The particle with the next highest energy inside the cone was combined with the first particle. The momenta of the combined particles were added and the direction of the sum was used to define a new cone, inside which the next highest energy particle was again looked for. This procedure was repeated until no more particles were found inside the cone. The resulting cone of particles was regarded as a $\tau$ candidate. Similarly, starting with the highest energy particle among the rest of the particles, a new cone of particles was searched for, until all the particles were finally assigned to a cone. Each $\tau$ candidate was then classified as a $\tau$ if it included at least one charged particle and its total energy exceeded 1% of the beam energy.

Events which had two cones of particles classified as a $\tau$ were selected as tau-pair events. The direction of each $\tau$ was approximated by that of the total momentum vector of its cone of particles and its charge was determined by the total charge in the cone. The acollinearity angle between the two $\tau$ momentum vectors was required to be less than 15 degrees, and the polar angle of each momentum vector was required to satisfy $|\cos\theta| < 0.85$.

These criteria provided a uniform selection efficiency within the angular region of $|\cos\theta| < 0.85$. A high degree of redundancy in the triggers enabled us to evaluate the trigger efficiency to be $99.8 \pm 0.1\%$. The total efficiency, including geometrical acceptance, was $67.8 \pm 2.5\%$ at $\sqrt{s} = M_Z$ and varied by 1% over the range of the energy scan.

The background contamination from multihadronic events was calculated to be $0.9 \pm 0.7\%$ using the JETSET Monte Carlo [9]. The remaining background from $\mu^+\mu^-$ events was estimated to be $0.7 \pm 0.4\%$ and that from cosmic rays and beam gas events to be $0.4 \pm 0.3\%$. The backgrounds from $e^+e^- \to e^+e^-$ and two-photon processes such as $e^+e^- \to e^+e^-e^+e^-$ were obtained by Monte Carlo simulations [8] and were $1.1 \pm 0.8\%$ and $0.4 \pm 0.4\%$ respectively. In total, the background in the sample amounted to $3.5 \pm 1.3\%$.

For the measurement of the forward-backward asymmetry, events in which the sign of the charge of each $\tau$ was the same were not used and at least one $\tau$ was required to have a charge of +1 or -1. Because of this, 2.1% of the sample was rejected, distributed uniformly in polar angle. From this number and a comparison with the Monte Carlo simulation, the forward-backward misassignment probability was found to be negligibly small ($< 0.1\%$). The effect of the background electron pair events on the asymmetry was evaluated from their angular distribution to be typically 0.005 and corrected accordingly. Effects from other backgrounds were negligible.

# 4 Results

Tables 1, 2 and 3 list the numbers of lepton pair events observed as functions of centre of mass energy, together with the corresponding luminosities. For the $e^+e^-$ events, the cross section is given after correction for the effects of efficiency and the kinematic cuts, as described in Section 3.1. For the $\mu^+\mu^-$ and $\tau^+\tau^-$ events the total cross sections, after all corrections for acceptance and efficiency, are given. These values were used in the fits.

The measured forward-backward charge asymmetries at different centre of mass energies are listed in Tables 4, 5 and 6. These have been evaluated by counting the numbers of events in the forward and backward polar angular regions, $N_{\rm F}$ and $N_{\rm B}$, and using the definition $A_{\rm FB} = (N_{\rm F} - N_{\rm B})/(N_{\rm F} + N_{\rm B})$. In each case the asymmetry is measured only within an experimentally limited polar angular acceptance region for each final state. For the $\mu^+\mu^-$ and $\tau^+\tau^-$ events, the forward and backward regions are defined in the normal way by $\cos\theta_{l^-} > 0$ and $\cos\theta_{l^-} < 0$. Because of the asymmetric acceptance cut used for the $e^+e^-$ events we define the "forward" region as $-0.15 < \cos\theta_{e^-} < 0.40$ and the "backward" region as $-0.70 < \cos\theta_{e^-} < -0.15$. These definitions, and the residual $t$-channel contributions, mean that the relationship between the $e^+e^-$ asymmetry and the effective axial vector and vector couplings is more complicated than it is for the $\mu^+\mu^-$ and $\tau^+\tau^-$ asymmetries. However, these effects are properly taken into account by the fitting procedure. Corrections are applied to the $e^+e^-$ asymmetry to account for the effects of the kinematic cuts, and to the $\tau^+\tau^-$ asymmetry to account for the $e^+e^-$ background.

These values of $A_{\rm FB}$ were used in the fits. The theoretical predictions for $A_{\rm FB}$, with these definitions and angular ranges, were calculated using the programs described in Section 5.

# 5 Analysis

## 5.1 Treatment of QED radiative corrections

Radiative corrections significantly modify the $e^+e^- \to l^+l^-$ cross sections and forward-backward asymmetries with respect to the tree level (Born) calculation. Photonic corrections, defined as the set of all diagrams incorporating an additional real or virtual photon with respect to the Born diagrams, form a gauge-invariant subset and can therefore be considered independently of other virtual corrections [10]. Photonic corrections are accounted for in such a way as not to affect the couplings to the $Z^0$.

For the parametrisation of the total and differential cross section of the $\mu^+\mu^-$ and $\tau^+\tau^-$ channels the routines MUCUT and MUCUTCOS provided in the program package ZBIZON [11] were used. In these programs photonic corrections are included as a complete $O(\alpha)$ calculation of initial and

final state radiation and their interference. Leading $O(\alpha^2)$ corrections and the exponentiation of soft photons are also included. The total cross section agrees with that obtained from the program ZSHAPE [12] to better than 0.2%. The effect of cuts on the differential cross section reproduces the results obtained with KORALZ [7] to better than 0.5% over the range of the energy scan.

The treatment of the $e^+e^- \to e^+e^-$ differential cross section is technically complicated by the presence of $t$-channel exchange diagrams. These diagrams are not included in the ZBIZON program [11] and we therefore used a parametrisation of the differential cross section for $e^+e^- \to e^+e^-(\gamma)$ based on the formulae given in references [13,14,15]. This includes contributions from lowest order and all one-loop and box diagrams associated with the $s$- and $t$-channel exchange of a $\gamma$ or $Z^0$ and all possible interference terms between them. Photonic corrections are treated to first order with the approximation that hard photons are considered only if they are emitted within an angle $\delta$ of a final-state lepton. The calculation also includes the exponentiation of soft photons.

The formalism developed in reference [13] and described in reference [14] is the basis of the $e^+e^-$ line shape program BHABHA [16]. The total cross section calculated from only the $s$-channel terms in BHABHA was compared with that predicted by the KORALZ Monte Carlo program [7], using equivalent input parameters. KORALZ includes photonic corrections up to $O(\alpha^2)$ with exponentiation of soft photons. The BHABHA program calculates a higher total cross section than the KORALZ program, with a 7% discrepancy at the $Z^0$ peak. Because of this we have modified the BHABHA program by implementing a new photonic correction formula based on reference [15]. This accounts for some leading second order terms which were neglected in references [13,14] and uses a different factorisation scheme. This improved analytic formula was used in the fits to the $e^+e^- \to e^+e^-$ data described in this paper.

Several checks have been performed to evaluate the accuracy of this improved parametrisation. The cross sections and forward-backward asymmetries calculated from the new formula, for $s$-channel exchange only, were again compared with those predicted by the KORALZ Monte Carlo program [7]. The cross sections obtained from the two programs agree to within 1.5% at the $Z^0$ peak and below. At the highest energies of the scan (93.3 and 94.3 GeV) the discrepancy between the two calculations of the cross section becomes more than 2%. For the forward-backward asymmetries the difference between the calculations of the new formula and the KORALZ program is less than 0.01. These discrepancies were taken as a measure of the systematic error in the calculation of the $s$-channel exchange diagrams by the improved analytic formula.

Since we have no sufficiently accurate $e^+e^- \to e^+e^-$ Monte Carlo program against which to check the $t$-channel calculation of the improved formula, we chose to reduce the contribution of the $t$-channel terms, which is especially important in the forward direction, by applying an asymmetric cut to define the $e^+e^-$ acceptance. The analysis was restricted to the range $-0.70 < \cos\theta_{e^-} < 0.40$. For this range, the contribution to the total $e^+e^-$ cross section from the sum of purely $t$-channel and $s$-$t$-channel interference terms is calculated by the improved analytic formula to be less than 4% at and above the $Z^0$ peak and 30% at 3 GeV below the peak. An arbitrary but conservative theoretical systematic error of 25% has been assigned to these remaining terms. However, this has little effect on the results, for the angular acceptance used and compared to our present statistical errors. When combined with the systematic uncertainty in the estimate of the $s$-channel exchange, it results in less than 2% systematic error in the total $e^+e^-$ cross section at the $Z^0$ peak and above. Below the $Z^0$ peak the systematic error increases as the energy decreases and reaches 9% at $\sqrt{s} = 88.3$ GeV. The systematic error on the $e^+e^-$ asymmetry is 0.01 at $\sqrt{s} = M_Z$ and 0.06 at $\sqrt{s} = 88.3$ GeV. These systematic errors were included as correlated errors in the fits for both the cross section and the forward-backward asymmetry measurements.

## 5.2 Results of the Fits

The fits are based on a $\chi^2$ minimisation procedure, which takes into account the full correlation matrix of the experimental uncertainties. In order to include our measurements of the $Z^0$ mass, $M_Z$, and total decay width, $\Gamma_Z$, and to account properly for the errors in those measurements and their correlation with the parameters extracted from the leptonic cross section and asymmetry measurements, our hadronic cross section data [1] are included in the fits and $M_Z$ and $\Gamma_Z$ are treated as free parameters. The hadronic partial width, $\Gamma_{had}$, is also a free parameter. The treatment of the process $e^+e^- \to$ hadrons is analogous to the one described in a previous publication [1]. However, the package ZBIZON is used to account for photonic corrections in order to ensure consistency with the treatment of $\mu^+\mu^-$ and $\tau^+\tau^-$ final states.

In a first approach to fitting the data, a parametrisation is used which assumes that the $Z^0$ has only vector and axial vector couplings to leptons and which leads to a differential cross section for $s$-channel exchange of the form:

$$\frac{2s}{\pi\alpha^2}\frac{d\sigma}{d\cos\theta}(e^+e^- \to l^+l^-) = C_{\gamma\gamma}(1+\cos^2\theta) + \mathrm{Re}\{\chi(s)\}\left[C^{(1)}_{\gamma Z}(1+\cos^2\theta) + C^{(2)}_{\gamma Z}\cos\theta\right] + |\chi(s)|^2\left[C^{(1)}_{ZZ}(1+\cos^2\theta) + C^{(2)}_{ZZ}\cos\theta\right] \quad (1)$$

with

$$\chi = \frac{G_F M_Z^2}{8\pi\alpha\sqrt{2}}\frac{s}{s - M_Z^2 + is\Gamma_Z/M_Z}$$

$G_F$ is the Fermi coupling constant and $\alpha$ is the fine structure constant.

In this expression the first term accounts for the pure photon exchange channel, the second term for $\gamma Z^0$ interference and the third for pure $Z^0$ exchange. At tree level the coefficients $C^{(1,2)}_{ZZ}$ and $C^{(1,2)}_{\gamma Z}$ are directly related to the vector and axial vector couplings of the $Z^0$ to leptons. This relationship is modified by higher order virtual corrections, which are sensitive to the detailed structure of the underlying theory. In general the higher order corrections introduce an $s$-dependence in the $C^{(1,2)}_{ZZ}$ and $C^{(1,2)}_{\gamma Z}$ coefficients. In the specific example of the Standard Model, however, the $s$-dependence of these coefficients is negligible and it is neglected in our fit.

In principle, the four coefficients $C^{(1,2)}_{\gamma Z}$ and $C^{(1,2)}_{ZZ}$ can be obtained from a fit to the measured differential cross sections and their energy dependence. In practice our present measurements of the leptonic cross sections and forward-backward asymmetries are used to extract the values of only the dominant coefficients, $C^{(1)}_{ZZ}$ and $C^{(2)}_{ZZ}$.

The parameter $C^{(1)}_{ZZ}$ determines the contribution to the cross section, integrated over $\cos\theta$, from the $s$-channel $Z^0$ exchange, which is dominant at $s = M_Z^2$. The forward-backward asymmetry at the peak is determined mainly by the ratio $C^{(2)}_{ZZ}/C^{(1)}_{ZZ}$. Universality is assumed between initial and final state leptons. Then, $C^{(1)}_{ZZ}$ can be rewritten as

$$C^{(1)}_{ZZ} = \left(\frac{24\pi\sqrt{2}}{G_F M_Z^3}\Gamma_{l^+l^-}\right)^2$$

where $\Gamma_{l^+l^-}$ is the partial decay width of the $Z^0$ to charged leptons, and $C_{ZZ}^{(2)}$ can be related to the square of the product of the effective axial vector coupling, $\hat{a}_l$, and the effective vector coupling, $\hat{v}_l$, of leptons to the $Z^0$, as defined in the improved Born approximation: $C_{ZZ}^{(2)} \equiv 8\hat{a}_l^2\hat{v}_l^2$ (see Equation (2) below and Reference [10]). Hence the fit to extract $C_{ZZ}^{(1)}$ and $C_{ZZ}^{(2)}$ can be reparametrised in terms of $\Gamma_{l^+l^-}$ and $\hat{a}_l^2\hat{v}_l^2$.

The remaining $\gamma Z^0$ interference terms in Equation (1) vanish at $s = M_Z^2$, in the absence of photonic corrections. In order to account properly in the fit for the energy dependence of the interference terms, $C_{\gamma Z}^{(1,2)}$ is reformulated in terms of $\Gamma_{l^+l^-}$, $\hat{a}_l^2$ and $\hat{v}_l^2$, in the framework of the improved Born approximation [10]. Constraints from the minimal Standard Model (see Equation (3) below) are used to derive $\hat{a}_l^2$ and $\hat{v}_l^2$ as functions of $\Gamma_{l^+l^-}$. This ansatz is also applied to the pure $t$-channel $Z^0$ exchange and the $s$-$t$-channel interference terms which contribute to the $e^+e^- \to e^+e^-$ differential cross section. The effect of varying $\hat{a}_l^2$ by a factor of 1.1 and $\hat{v}_l^2$ by up to a factor 10 with respect to the values assigned to them by this procedure does not significantly affect the quality of the fits and does not bias the results obtained for $\Gamma_{l^+l^-}$ and $\hat{a}_l^2\hat{v}_l^2$.

Firstly, each of the $e^+e^-$, $\mu^+\mu^-$ and $\tau^+\tau^-$ final states is fitted separately. In each case universality between initial and final state leptons is assumed. The results of these fits are summarised in Table 7, columns 1-3. The values of $\Gamma_{l^+l^-}$ and $\hat{a}_l^2\hat{v}_l^2$ for the three lepton types are consistent with each other, supporting the principle of lepton universality. Therefore the fit is repeated combining the data for the three lepton modes. Figures 1 and 2 show the corrected cross sections and forward-backward asymmetries as functions of $\sqrt{s}$, together with the corresponding fitted curves. The results of this fit are given in Table 7, column 4. Because of the difficulties involved in the analysis of the $e^+e^- \to e^+e^-$ channel a fit has been made, for the purpose of comparison, using only the $\mu^+\mu^-$ and $\tau^+\tau^-$ data. The results are given in Table 7, column 5, and are consistent with those in column 4. Therefore, for the subsequent fits, all our data are included and lepton universality is assumed.

These results are consistent with those from an earlier analysis of this data [1] (see Section 6) and also with measurements made by other experiments [17-22].

In Figure 3 the confidence level contours of our result are shown in the $\hat{a}_l^2\hat{v}_l^2$ vs. $\Gamma_{l^+l^-}$ plane. Also shown is the Standard Model prediction for these two parameters, allowing the masses of the top quark, $m_t$, and of the Higgs particle, $M_{\mathrm{H}}$, to vary within the range $50 < m_t < 250$ GeV/$c^2$ and $20 < M_{\mathrm{H}} < 1000$ GeV/$c^2$. The measured values are in good agreement with the Standard Model prediction for all values of $m_t$ and $M_{\mathrm{H}}$ considered here.

The measured leptonic cross sections and forward-backward asymmetries can be expressed directly in terms of effective axial vector and vector coupling constants, $\hat{a}_l^2$ and $\hat{v}_l^2$. In order to extract $\hat{a}_l^2$ and $\hat{v}_l^2$ the differential cross section (1) is rewritten in the form of the improved Born approximation [10]:

$$\frac{2s}{\pi\alpha^2}\frac{d\sigma}{d\cos\theta}(e^+e^- \to l^+l^-) = \left(\frac{1}{1-\Delta\alpha}\right)^2(1+\cos^2\theta) + \frac{2}{1-\Delta\alpha}\mathrm{Re}\{\chi(s)\}\left[\hat{v}_l^2(1+\cos^2\theta) + 2\hat{a}_l^2\cos\theta\right]$$
$$+ |\chi(s)|^2\left[(\hat{a}_l^2+\hat{v}_l^2)^2(1+\cos^2\theta) + 8\hat{a}_l^2\hat{v}_l^2\cos\theta\right] \qquad (2)$$

$\Delta\alpha$ is the QED vacuum polarisation correction. This formulation assumes the tree level relationship between the coefficients $C_{ZZ}^{(1,2)}$ and $C_{\gamma Z}^{(1,2)}$. In order to account for the possibility of a negative forward-backward asymmetry at $s = M_Z^2$, negative values of $\hat{v}_l^2$ are allowed. The constraints $\hat{a}_l^2 > 0$ and $\hat{a}_l^2 > \hat{v}_l^2$ are imposed, since this is known from earlier measurements of the axial vector coupling [23-25].

The results from this fit are given in Table 8, column 1. The value of $\hat{a}_l^2$ is determined mainly by the cross section measurements and the value of $\hat{v}_l^2$ mainly by the asymmetry measurements. They are consistent with previous measurements from $Z^0$ decays [21,22] and also with those from lower energy $e^+e^-$ colliders [23], neutrino-electron scattering experiments [24] and other measurements [25]. It is not possible to determine the signs of $\hat{a}_l$ and $\hat{v}_l$ using our data alone.

Alternatively the differential cross section may be reparametrised in terms of $\rho_Z$ and an effective weak mixing angle $\sin^2\overline{\theta}_W$ [26] by substituting in (2) the following expressions for the coupling constants:

$$\hat{a}_l^2 \to \rho_Z \qquad \text{and} \qquad \hat{v}_l^2 \to \rho_Z(1 - 4\sin^2\overline{\theta}_W)^2.$$

Note that this parametrisation cannot accommodate negative values for the forward-backward asymmetry at $s = M_Z^2$. The results of this fit are given in Table 8, column 2. Figure 4 shows the one standard deviation confidence level contour in the $\rho_Z$ vs. $\sin^2\overline{\theta}_W$ plane. Because $\hat{v}_l$ enters only quadratically in the improved Born approximation, the confidence level contour obtained from the fit is symmetric about the axis $\sin^2\overline{\theta}_W = 0.25$. The stars indicate our best fitted values:

$$\rho_Z = 0.998 \pm 0.024 \qquad \text{and} \qquad \sin^2\overline{\theta}_W = 0.233^{+0.045}_{-0.012},$$

where the value of $\sin^2\overline{\theta}_W < 0.25$ has been chosen.

In this fit, $\rho_Z$ is determined mainly by the cross section measurements and $\sin^2\overline{\theta}_W$ mainly by the asymmetry measurements. These can be combined, to give a more precise value of $\sin^2\overline{\theta}_W$, by making use of the approximate relationship between $\rho_Z$ and $\sin^2\overline{\theta}_W$ in the Standard Model, with minimal Higgs structure [10]:

$$\sin^2\overline{\theta}_W^{SM} = \frac{1}{2}\left(1 - \sqrt{1 - \frac{4A}{\rho_Z M_Z^2(1-\Delta\alpha)}}\right) \tag{3}$$

where $A = (\pi\alpha)/(\sqrt{2}G_F)$. The results of a fit with this constraint imposed are given in Table 8, column 3. For the effective weak mixing angle we obtain:

$$\sin^2\overline{\theta}_W^{SM} = 0.233\ ^{+0.007}_{-0.006} \pm 0.002$$

where the first error quoted is experimental and the second is theoretical.

Although this value of $\sin^2\overline{\theta}_W^{SM}$ is obtained from a fit to both the leptonic asymmetry and cross section measurements, it is determined mainly by the latter, that is by the value of $\Gamma_{l^+l^-}$. The theoretical error quoted was estimated as follows. The full one loop calculation was used to obtain values for $\sin^2\overline{\theta}_W^{SM}$ and $\Gamma_{l^+l^-}^{SM}$ over the range of $m_t$ and $M_H$ given above. The value of $\sin^2\overline{\theta}_W^{SM}$ was compared with that derived from $\Gamma_{l^+l^-}^{SM}$ using the improved Born approximation with the Standard Model constraint (3) and the discrepancy between the two calculations was taken as the measure of the theoretical error.

In Figure 4, the dash-dotted line indicates the minimal Standard Model relationship (3) between $\rho_Z$ and $\sin^2\overline{\theta}_W^{SM}$. Symbols on this line refer to values corresponding to various choices of $m_t$ and $M_H$. Also indicated as an error bar in Figure 4 is our result for $\sin^2\overline{\theta}_W^{SM}$. Our results are consistent with previous measurements of the weak mixing angle [18,23-28]. See reference [26] for a comparison of the different definitions and measurements of $\sin^2\theta_W$.

# 6 Update of Combined Analysis of Hadronic and Leptonic Data

In a recent publication [1] we presented combined fits to cross section measurements as functions of centre of mass energy for $Z^0$ decays into hadronic and leptonic final states. Values were extracted for the $Z^0$ total width and its partial decay widths into hadrons and leptons. We derived values for the ratio of the hadronic to the leptonic partial width, $R_Z \equiv \Gamma_{had}/\Gamma_{l^+l^-} = 22.43 \pm 0.75$; the partial decay width of the $Z^0$ into invisible final states, $\Gamma_{inv} = 453 \pm 44$ MeV, and the number of light neutrino species, $N_\nu \equiv \Gamma_{inv}/\Gamma_\nu^{SM} = 2.73 \pm 0.26(exp)^{+0.02}_{-0.04}(theor)$, assuming the Standard Model value of $\Gamma_\nu^{SM} = 166.2^{+2.7}_{-0.7}$ MeV for the partial decay width into a single light neutrino species.

Because our hadronic data are included in the fits presented in this paper, the new results for the partial widths represent an update to those given in [1]. There are two improvements compared to the previous analysis.

Firstly, the data sample for the $\mu^+\mu^-$ and $\tau^+\tau^-$ final states has been enlarged by extending the acceptance out from $|\cos\theta| < 0.70$ to $|\cos\theta| < 0.82$ and $|\cos\theta| < 0.85$ respectively. For the $\tau^+\tau^-$ events the selection efficiency has also been increased. Secondly, an improved parametrisation of the $e^+e^-$ line shape has been used, as described in Section 5.1.

Our updated results, using $e^+e^-$, $\mu^+\mu^-$, $\tau^+\tau^-$ and hadronic data, are: $R_Z = 21.72^{+0.71}_{-0.65}$, $\Gamma_{inv} = 474 \pm 43$ MeV and $N_\nu = 2.85 \pm 0.26(exp)^{+0.02}_{-0.04}(theor)$. The changes relative to the previously published values arise mainly from the use of a different $e^+e^-$ line shape parametrisation.

Excluding the $e^+e^-$ data, in order to avoid the difficulties introduced by the $t$-channel contributions, we obtain from our $\mu^+\mu^-$, $\tau^+\tau^-$ and hadronic data $R_Z = 22.11^{+0.84}_{-0.74}$.

These results are consistent with the Standard Model with three light neutrino generations, and with measurements made by other experiments [17-21]. The Standard Model prediction for $R_Z$ is $20.6 < R_Z^{SM} < 21.1$, where the range results from a variation of $m_t$ between 50 and 250 GeV/$c^2$, $M_H$ between 20 and 1000 GeV/$c^2$ and the strong coupling constant, $\alpha_s$, between 0.09 and 0.15. Our measurement is within 1.0 to 1.7 (excluding $e^+e^-$, 1.4 to 2.0) standard deviations of the Standard Model prediction.

# 7 Summary

Using all the data recorded by the OPAL detector during 1989 an extended analysis of the reactions $e^+e^- \to e^+e^-$, $e^+e^- \to \mu^+\mu^-$ and $e^+e^- \to \tau^+\tau^-$ has been made at several centre of mass energies around the $Z^0$ mass. The cross sections and forward-backward asymmetries have been measured and used to determine the couplings of the $Z^0$ to charged leptons. The data are consistent with lepton universality.

Using the parametrisation (1) of the differential cross section, the charged leptonic partial decay width of the $Z^0$ is found to be $\Gamma_{l^+l^-} = 83.1 \pm 1.9$ MeV and the square of the product of the effective axial vector and vector coupling constants of the $Z^0$ to charged leptons is $\hat{a}_l^2\hat{v}_l^2 = 0.0039 \pm 0.0083$, in agreement with the Standard Model expectation.

From a parametrisation in terms of the improved Born approximation the effective axial vector and vector coupling constants are determined to be $\hat{a}_l^2 = 0.998 \pm 0.024$ and $\hat{v}_l^2 = 0.0044 \pm 0.0083$.

Equivalently, in the framework of the Standard Model, the parameters $\rho_Z$ and $\sin^2\overline{\theta}_W$ are $0.998 \pm 0.024$ and $0.233^{+0.045}_{-0.012}$ respectively.

In the minimal Standard Model, in which $\rho_Z$ and $\sin^2\overline{\theta}_W$ are related, $\sin^2\overline{\theta}_W^{SM}$ is found to be $0.233^{+0.007}_{-0.006} \pm 0.002$, where the first error is experimental and the second is theoretical.

Our previously published value for the ratio of the hadronic to the charged leptonic partial decay width of the $Z^0$ has been updated, giving $R_Z = 21.72^{+0.71}_{-0.65}$, which is within about 1.5 standard deviations of the Standard Model prediction.

# 8 Acknowledgements

We are grateful to M. Greco for his help and advice concerning the analytic formula used in the analysis of the $e^+e^- \to e^+e^-$ data.

It is a pleasure to thank the SL Division for the efficient operation of the machine, the precise information on the absolute energy, and their continuing close cooperation with our experimental group. In addition to the support staff at our own institutions we are pleased to acknowledge the following: The Bundesministerium für Forschung und Technologie, FRG; The Department of Energy, USA; The Institut de Recherche Fondamentale du Commissariat a l'Energie Atomique; The Israeli Ministry of Science; The Minerva Gesellschaft; The National Science Foundation, USA; The Natural Sciences and Engineering Research Council, Canada; The Japanese Ministry of Education, Science and Culture (the Monbusho) and a grant under the Monbusho International Science Research Program; The American Israeli Bi-national Science Foundation; The Science and Engineering Research Council, UK and The A. P. Sloan Foundation.

## References


[1] OPAL Collaboration, M.Z. Akrawy et al., Phys. Lett. B240 (1990) 497.

[2] OPAL Technical proposal (1983) and CERN/LEPC/83-4;
OPAL Collaboration, K. Ahmet et al., The OPAL Detector at LEP,
to be submitted to Nucl. Instr. and Meth.

[3] OPAL Collaboration, M.Z. Akrawy et al., Phys. Lett. B231 (1989) 530.

[4] OPAL Collaboration, M.Z. Akrawy et al., Phys. Lett. B235 (1990) 379.

[5] J. Allison et al., Comp. Phys. Comm. 47 (1987) 55;
R. Brun et al., GEANT 3, Report DD/EE/84-1, CERN (1989).

[6] M. Böhm, A. Denner and W. Hollik, Nucl. Phys. B304 (1988) 687;
F.A. Berends, R. Kleiss, W. Hollik, Nucl. Phys. B304 (1988) 712.

[7] S. Jadach et al., Z Physics at LEP1, CERN 89-08, ed. G. Altarelli et al., Vol 1 (1989) 235;
KORALZ, Version 37.

[8] F.A. Berends, P.H. Daverveldt and R. Kleiss, Comp. Phys. Comm. 40 (1986) 271, 285, 309.

[9] T. Sjöstrand, Comp. Phys. Comm. 39 (1986) 347; JETSET, Version 7.1.

[10] M. Consoli and W. Hollik, Z Physics at LEP1, CERN 89-08, ed. G. Altarelli et al., Vol 1 (1989) 7.

[11] Line shape program ZBIZON, Dubna-Zeuthen radiative correction group, D. Bardin et al.

[12] Line shape program ZSHAPE, W.J.P. Beenakker, F.A. Berends and S.C. van der Merk (Institut-Lorentz, University of Leiden, POB 9506, 2300 RA Leiden, The Netherlands)

[13] M. Greco, Phys. Lett. B177 (1986) 97.

[14] M. Caffo, E. Remiddi and F. Semeria, Z Physics at LEP1, CERN 89−08, ed. G. Altarelli et al., Vol.1 (1989) 171.

[15] F. Aversa and M. Greco, Phys. Lett. B228 (1989) 134;
M. Greco, private communication;
F. Aversa et al., paper in preparation.

[16] Program BHABHA from M. Caffo, E. Remiddi and F. Semeria, version of 12 February 1990.

[17] Mark II Collaboration, G.S. Abrams et al., Phys. Rev. Lett. 63 (1989) 2173.

[18] ALEPH Collaboration, D. Decamp et al., Phys. Lett. B235 (1990) 399.

[19] L3 Collaboration, B. Adeva et al., Phys. Lett. B237 (1990) 136.

[20] DELPHI Collaboration, P. Aarnio et al., Phys. Lett. B241 (1990) 425;
DELPHI Collaboration, P. Abreu et al., Phys. Lett. B241 (1990) 435.

[21] Mark II Collaboration, G.S. Abrams et al., Phys. Rev. Lett. 63 (1989) 2780.

[22] L3 Collaboration, B. Adeva et al., Phys. Lett. B236 (1990) 109;
L3 Collaboration, B. Adeva et al., Phys. Lett. B238 (1990) 122.

[23] HRS Collaboration, M. Derrick et al., Phys. Rev. D31 (1985) 2352,
HRS Collaboration, K.K. Gan et al, Phys. Lett. 153B (1985) 116;
MAC Collaboration, E. Fernandez et al, Phys. Rev. D35 (1987) 10,
MAC Collaboration, W.W. Ash et al, Phys. Rev. Lett. 55 (1985) 1831,
MAC Collaboration, E. Fernandez et al, Phys. Rev. Lett. 54 (1985) 1620;
Mark II Collaboration, M.E. Levi et al, Phys. Rev. Lett. 51 (1983) 1941;
CELLO Collaboration, H.-J. Behrend et al., Phys. Lett. B191 (1987) 209,
CELLO Collaboration, H.-J. Behrend et al., Phys. Lett. B222 (1989) 163;
JADE Collaboration, S. Hegner et al., Z. Phys. C46 (1990) 547;
MarkJ Collaboration, B. Adeva et al., Phys. Rev. D38 (1988) 2665;
PLUTO Collaboration, Ch. Berger et al., Z. Phys. C27 (1985) 341,
PLUTO Collaboration, Ch. Berger et al., Z. Phys. C28 (1985) 1;
TASSO Collaboration, W. Braunschweig et al., Z. Phys. C40 (1988) 163
(erratum Z. Phys. C42 (1989) 348),
TASSO Collaboration, W. Braunschweig et al., Z. Phys. C43 (1989) 549;
AMY Collaboration, A. Bacala et al., Phys. Lett. B218 (1989) 112;
TOPAZ Collaboration, I. Adachi et al., Phys. Lett. B208 (1988) 319;
VENUS Collaboration, K. Abe et al., KEK preprint 89-192 (1990), submitted to Z. Phys. C;
A. Maki, Proceedings of the 1989 International Symposium on Lepton and Photon Interactions at High Energies, Stanford University, August 7-12, 1989, p. 203.

[24] CHARM Collaboration, J. Dorenbosch et al., Z. Phys. C41 (1989) 567;
K. Abe et al., Phys. Rev. Lett. 62 (1989) 1709;
CHARM-II Collaboration, D. Geiregat et al., Phys. Lett. B232 (1989) 539.

[25] For summaries of earlier results see:
U. Amaldi et al., Phys. Rev. D36 (1987) 1385;
G. Costa et al., Nucl. Phys. B297 (1988) 244;
G.L. Fogli and D. Haidt, Z. Phys. C40 (1988) 379;
Particle Data Group, G.P. Yost et al, Phys. Lett. B204 (1988) 1.

[26] G. Altarelli, Proceedings of the 1989 International Symposium on Lepton and Photon Interactions at High Energies, Stanford University, August 7-12, 1989, p. 286.

[27] CHARM Collaboration, J.V. Allaby et al., Z. Phys. C36 (1987) 611;
A. Blondel et al., Z. Phys. C45 (1990) 361.

[28] UA2 Collaboration, J. Alitti et al., Phys. Lett. B241 (1990) 150.

# Figure Captions

Figure 1: Cross sections as functions of centre of mass energy for: a) $e^+e^- \to e^+e^-$, integrated over $-0.7 < \cos\theta_{e^-} < 0.4$; b) $e^+e^- \to \mu^+\mu^-$, corrected for acceptance; c) $e^+e^- \to \tau^+\tau^-$, corrected for acceptance; d) $e^+e^- \to$ hadrons, corrected for acceptance. The solid lines are the results of the fit to the combined $e^+e^-$, $\mu^+\mu^-$, $\tau^+\tau^-$ and hadronic data described in the text.

Figure 2: Forward-backward charge asymmetries for: a) $e^+e^- \to e^+e^-$, within $-0.7 < \cos\theta_{e^-} < 0.4$; b) $e^+e^- \to \mu^+\mu^-$, within $|\cos\theta| < 0.82$; c) $e^+e^- \to \tau^+\tau^-$, within $|\cos\theta| < 0.85$. For the $e^+e^-$ case, the "forward" and "backward" cross sections are defined in the polar angular regions $-0.15 < \cos\theta_{e^-} < 0.4$ and $-0.7 < \cos\theta_{e^-} < -0.15$ respectively. The solid lines are the results of the fit to the combined $e^+e^-$, $\mu^+\mu^-$, $\tau^+\tau^-$ and hadronic data described in the text.

Figure 3: One and two standard deviation confidence level contours in the $\hat{a}_l^2\hat{v}_l^2$ vs. $\Gamma_{l^+l^-}$ plane. The star indicates our best fitted values. The region inside the solid line corresponds to the Standard Model prediction for $50 < m_t < 250$ GeV/$c^2$ and $20 < M_{\rm H} < 1000$ GeV/$c^2$.

Figure 4: One standard deviation confidence level contour in the $\rho_{\rm Z}$ vs. $\sin^2\overline{\theta}_{\rm W}$ plane. The stars indicate our best fitted values for $\rho_{\rm Z}$ and $\sin^2\overline{\theta}_{\rm W}$. There are two solutions, symmetric about $\sin^2\overline{\theta}_{\rm W} = 0.25$. The dash-dotted line shows the minimal Standard Model relationship between $\rho_{\rm Z}$ and $\sin^2\overline{\theta}_{\rm W}$, with symbols indicating various choices of $m_t$ and $M_{\rm H}$ in GeV/$c^2$. The error bar shows our one standard deviation limits on $\sin^2\overline{\theta}_{\rm W}^{\rm SM}$ after applying this minimal Standard Model constraint.

| $\sqrt{s}$ (GeV) | Luminosity ($nb^{-1}$) | $N_{ee}$ | $\sigma_{ee}^{corr}$ (nb) |
|---|---|---|---|
| 88.28 | $113.9 \pm 1.6$ | 16 | $0.143 \pm 0.039$ |
| 89.28 | $60.3 \pm 1.2$ | 15 | $0.253 \pm 0.068$ |
| 90.28 | $107.4 \pm 1.6$ | 51 | $0.484 \pm 0.071$ |
| 91.03 | $192.4 \pm 2.2$ | 109 | $0.577 \pm 0.056$ |
| 91.28 | $217.1 \pm 2.3$ | 146 | $0.685 \pm 0.059$ |
| 91.53 | $195.9 \pm 2.2$ | 123 | $0.640 \pm 0.058$ |
| 92.28 | $74.8 \pm 1.4$ | 32 | $0.435 \pm 0.077$ |
| 93.28 | $109.2 \pm 1.7$ | 27 | $0.250 \pm 0.048$ |
| 94.28 | $84.0 \pm 1.5$ | 19 | $0.225 \pm 0.052$ |

Table 1: The cross section for $e^+e^- \to e^+e^-$, from a total of 538 events. $\sigma_{ee}^{corr}$ is the cross section measured within the angular acceptance $-0.7 < \cos\theta_{e^-} < 0.4$ and corrected for the effects of efficiency and the kinematic cuts, as described in Section 3.1. The errors quoted are the results of combining in quadrature the statistical errors with the systematic errors assigned to the analytic formula, as described in Section 5.1.

| $\sqrt{s}$ (GeV) | Luminosity ($nb^{-1}$) | $N_{\mu\mu}$ | $\sigma_{\mu\mu}^{tot}$ (nb) |
|---|---|---|---|
| 88.28 | $113.6 \pm 1.6$ | 24 | $0.283 \pm 0.058$ |
| 89.28 | $41.7 \pm 1.0$ | 11 | $0.352 \pm 0.106$ |
| 90.28 | $78.7 \pm 1.4$ | 53 | $0.889 \pm 0.123$ |
| 91.03 | $157.9 \pm 2.0$ | 148 | $1.238 \pm 0.102$ |
| 91.28 | $160.5 \pm 2.0$ | 179 | $1.467 \pm 0.110$ |
| 91.53 | $190.8 \pm 2.2$ | 198 | $1.366 \pm 0.098$ |
| 92.28 | $53.7 \pm 1.2$ | 40 | $0.988 \pm 0.157$ |
| 93.28 | $85.4 \pm 1.5$ | 35 | $0.549 \pm 0.093$ |
| 94.28 | $79.2 \pm 1.4$ | 25 | $0.422 \pm 0.085$ |

Table 2: The cross section for $e^+e^- \to \mu^+\mu^-$, from a total of 713 events. $\sigma_{\mu\mu}^{tot}$ is the total cross section after correction for efficiency and acceptance. The quoted errors are statistical only.

| $\sqrt{s}$ (GeV) | Luminosity ($nb^{-1}$) | $N_{\tau\tau}$ | $\sigma_{\tau\tau}^{tot}$ (nb) |
|---|---|---|---|
| 88.28 | $110.9 \pm 1.6$ | 20 | $0.262 \pm 0.059$ |
| 89.29 | $56.1 \pm 1.2$ | 14 | $0.360 \pm 0.096$ |
| 90.28 | $92.9 \pm 1.5$ | 56 | $0.864 \pm 0.116$ |
| 91.03 | $174.6 \pm 2.1$ | 180 | $1.471 \pm 0.111$ |
| 91.29 | $157.7 \pm 2.0$ | 151 | $1.367 \pm 0.112$ |
| 91.53 | $178.4 \pm 2.1$ | 181 | $1.448 \pm 0.109$ |
| 92.29 | $56.3 \pm 1.2$ | 34 | $0.864 \pm 0.149$ |
| 93.29 | $99.2 \pm 1.6$ | 41 | $0.593 \pm 0.093$ |
| 94.28 | $78.1 \pm 1.4$ | 18 | $0.331 \pm 0.078$ |

Table 3: The cross section for $e^+e^- \to \tau^+\tau^-$, from a total of 695 events. $\sigma_{\tau\tau}^{tot}$ is the total cross section after correction for efficiency and acceptance. The quoted errors are statistical only.

| $\sqrt{s}$ (GeV) | $N_F^{ee}$ | $N_B^{ee}$ | $A_{FB}^{ee\ corr}$ |
|---|---|---|---|
| 88.28 | 8 | 10 | $-0.11 \pm 0.23$ |
| 89.28 | 8 | 10 | $-0.11 \pm 0.23$ |
| 90.28 | 32 | 24 | $0.14 \pm 0.13$ |
| 91.03 | 65 | 61 | $0.03 \pm 0.09$ |
| 91.28 | 70 | 93 | $-0.14 \pm 0.08$ |
| 91.53 | 65 | 75 | $-0.07 \pm 0.08$ |
| 92.28 | 15 | 19 | $-0.12 \pm 0.17$ |
| 93.28 | 15 | 15 | $0.00 \pm 0.18$ |
| 94.32 | 8 | 13 | $-0.23 \pm 0.21$ |

Table 4: The forward-backward asymmetry for $e^+e^- \to e^+e^-$ within $-0.70 < \cos\theta_{e^-} < 0.40$, from a total of 606 events. "Forward" is defined as $-0.15 < \cos\theta_{e^-} < 0.40$ and "backward" as $-0.70 < \cos\theta_{e^-} < -0.15$. $A_{FB}^{ee\ corr}$ is the asymmetry after correction for the effects of the kinematic cuts, as described in Section 3.1. The errors quoted are the results of combining in quadrature the statistical errors with the systematic errors assigned to the analytic formula, as described in Section 5.1.

| $\sqrt{s}$ (GeV) | $N_F^{\mu\mu}$ | $N_B^{\mu\mu}$ | $A_{FB}^{\mu\mu}$ |
|---|---|---|---|
| 88.28 | 12 | 12 | $0.00 \pm 0.20$ |
| 89.28 | 7 | 9 | $-0.13 \pm 0.25$ |
| 90.28 | 36 | 43 | $-0.09 \pm 0.11$ |
| 91.04 | 79 | 98 | $-0.11 \pm 0.08$ |
| 91.29 | 117 | 115 | $0.01 \pm 0.07$ |
| 91.53 | 116 | 91 | $0.12 \pm 0.07$ |
| 92.31 | 34 | 31 | $0.05 \pm 0.12$ |
| 93.29 | 29 | 23 | $0.12 \pm 0.14$ |
| 94.40 | 16 | 22 | $-0.16 \pm 0.16$ |

Table 5: The forward-backward asymmetry for $e^+e^- \to \mu^+\mu^-$ within $|\cos\theta| < 0.82$, from a total of 890 events. The quoted errors are statistical only.

| $\sqrt{s}$ (GeV) | $N_F^{\tau\tau}$ | $N_B^{\tau\tau}$ | $A_{FB}^{\tau\tau}$ |
|---|---|---|---|
| 88.28 | 10 | 12 | $-0.13 \pm 0.21$ |
| 89.28 | 6 | 11 | $-0.32 \pm 0.23$ |
| 90.28 | 32 | 31 | $0.01 \pm 0.13$ |
| 91.03 | 109 | 106 | $0.01 \pm 0.07$ |
| 91.28 | 110 | 108 | $0.01 \pm 0.07$ |
| 91.52 | 109 | 92 | $0.08 \pm 0.07$ |
| 92.30 | 32 | 31 | $-0.01 \pm 0.13$ |
| 93.28 | 25 | 22 | $0.06 \pm 0.15$ |
| 94.37 | 16 | 9 | $0.27 \pm 0.19$ |

Table 6: The forward-backward asymmetry for $e^+e^- \to \tau^+\tau^-$ within $|\cos\theta| < 0.85$, from a total of 871 events. A correction was applied for the contribution from the $e^+e^-$ background. The quoted errors are statistical only.

| | $e^+e^-$ | $\mu^+\mu^-$ | $\tau^+\tau^-$ | $e^+e^-$, $\mu^+\mu^-$, $\tau^+\tau^-$ | $\mu^+\mu^-$, $\tau^+\tau^-$ |
|---|---|---|---|---|---|
| $\Gamma_{l^+l^-}$ [MeV] | 84.5 ±3.1 | 81.9 ±2.4 | 82.6±2.6 | 83.1±1.9 | 82.2 ±2.1 |
| $\hat{a}_l^2\hat{v}_l^2$ | -0.0128±0.0246 | 0.0031±0.0127 | 0.0116±0.0126 | 0.0039±0.0083 | 0.0075±0.0089 |
| $M_Z$ [GeV] | 91.147±0.022 | 91.145±0.022 | 91.142±0.022 | 91.151±0.021 | 91.146±0.021 |
| $\Gamma_Z$ [GeV] | 2.534±0.046 | 2.530±0.046 | 2.519±0.046 | 2.527±0.044 | 2.524±0.045 |
| $\Gamma_{had}$ [GeV] | 1.775±0.065 | 1.830±0.056 | 1.801±0.060 | 1.804±0.044 | 1.817±0.048 |
| $\chi^2$ /NDOF | 16.9/24 | 17.3/24 | 14.1/24 | 37.4/60 | 23.9/42 |

Table 7: Results of the fits to the lepton pair cross sections and forward-backward asymmetries using the parametrisation (1) of the differential cross section described in Section 5.2. In each case universality has been assumed between initial and final state leptons. The hadronic cross section measurements are also included in every fit. $M_Z$ has an additional error of 30 MeV from the beam energy uncertainty.

| | $\hat{a}_l^2$, $\hat{v}_l^2$ fit | $\rho_Z$, $\sin^2\bar{\theta}_W$ fit | $\sin^2\bar{\theta}_W^{SM}$ fit |
|---|---|---|---|
| $\hat{a}_l^2$ | 0.998 ±0.024 | | |
| $\hat{v}_l^2$ | 0.0044±0.0083 | | |
| $\rho_Z$ | | 0.998±0.024 | |
| $\sin^2\bar{\theta}_W$ | | $0.233^{+0.045}_{-0.012}$ | $0.233^{+0.007}_{-0.006}$ |
| $M_Z$ [GeV] | 91.151±0.021 | 91.151±0.021 | 91.151±0.021 |
| $\Gamma_Z$ [GeV] | 2.527±0.044 | 2.527±0.044 | 2.526±0.042 |
| $\Gamma_{had}$ [GeV] | 1.804±0.045 | 1.804±0.045 | 1.803±0.044 |
| $\chi^2$ /NDOF | 37.4/60 | 37.4/60 | 37.4/61 |

Table 8: Results of the fits to the combined $e^+e^-$, $\mu^+\mu^-$ and $\tau^+\tau^-$ cross sections and forward-backward asymmetries based on the improved Born approximation (2), as described in Section 5.2. Lepton universality has been assumed. The hadronic cross section measurements are also included in every fit. In the $\rho_Z$, $\sin^2\bar{\theta}_W$ fit, the value of $\sin^2\bar{\theta}_W < 0.25$ has been chosen from the two possible solutions, which are symmetric about $\sin^2\bar{\theta}_W = 0.25$. $M_Z$ has an additional error of 30 MeV from the beam energy uncertainty. $\sin^2\bar{\theta}_W^{SM}$ has an additional theoretical uncertainty of 0.002.

# Figure 1

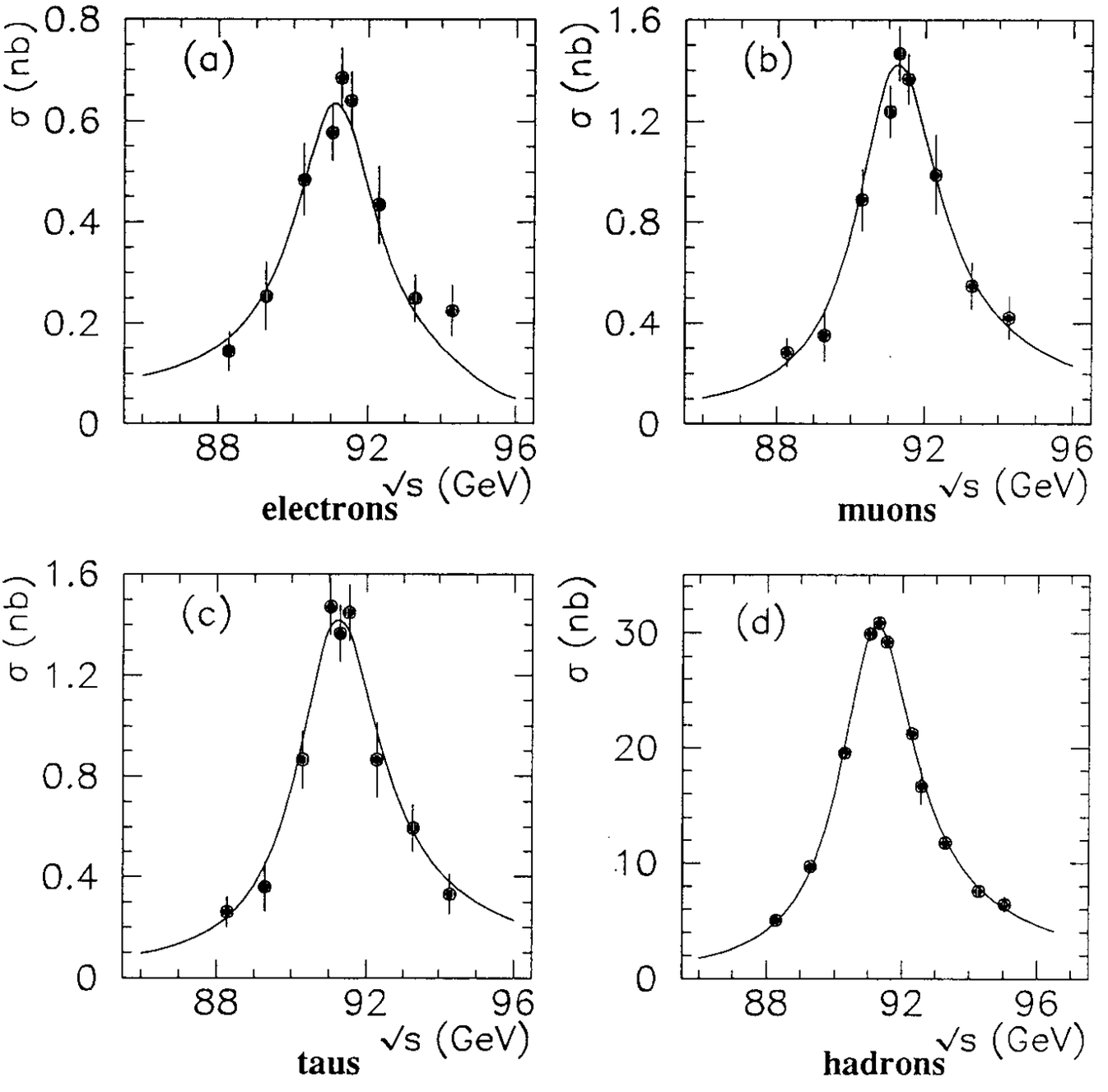
(a)
σ (nb)
0.8
0.6
0.4
0.2
0
88
92
96
√s (GeV)
electrons
(b)
σ (nb)
1.6
1.2
0.8
0.4
0
88
92
96
√s (GeV)
muons
(c)
σ (nb)
1.6
1.2
0.8
0.4
0
88
92
96
√s (GeV)
taus
(d)
σ (nb)
30
20
10
0
88
92
96
√s (GeV)
hadrons

# Figure 2

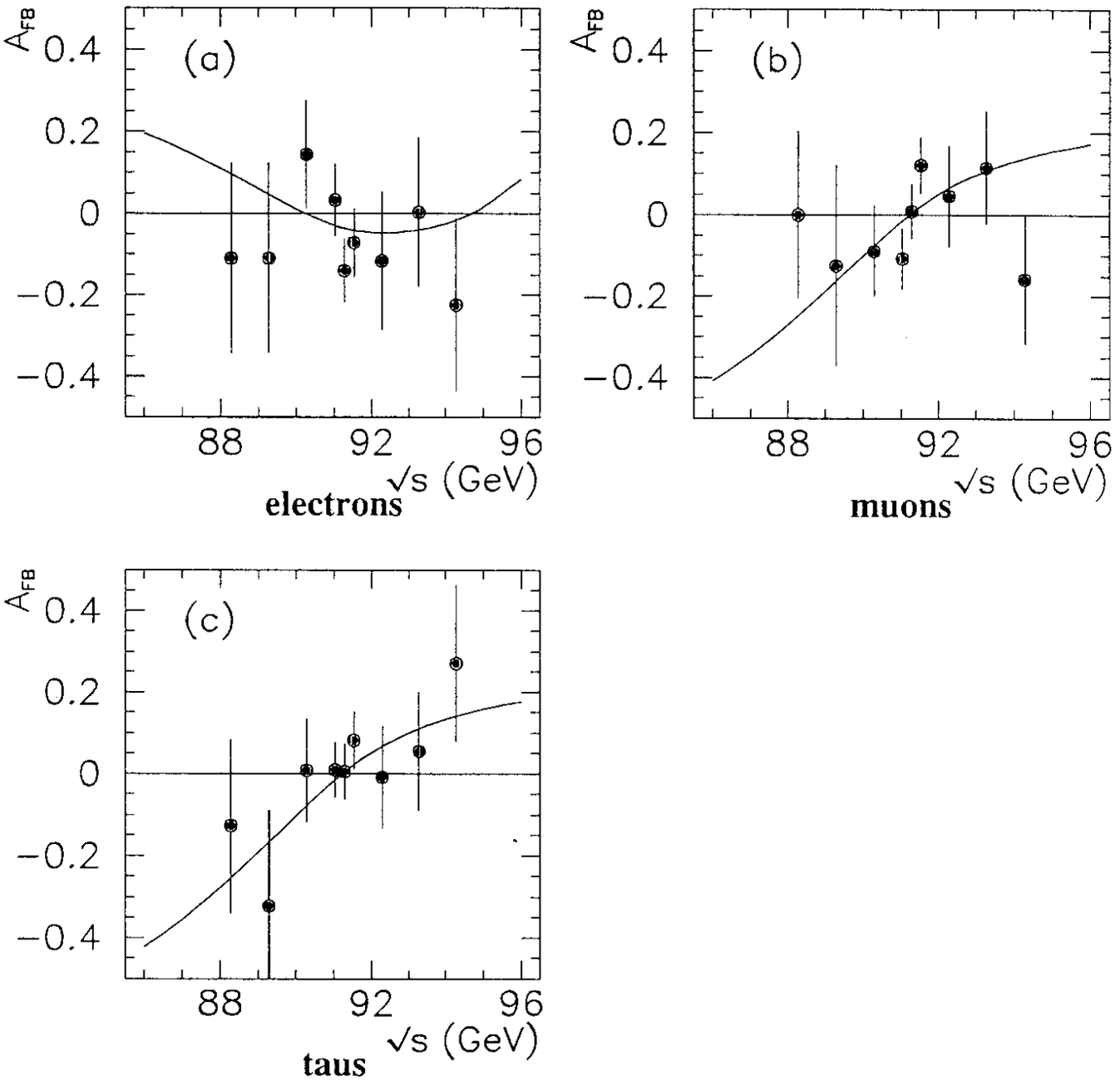

# Figure 3

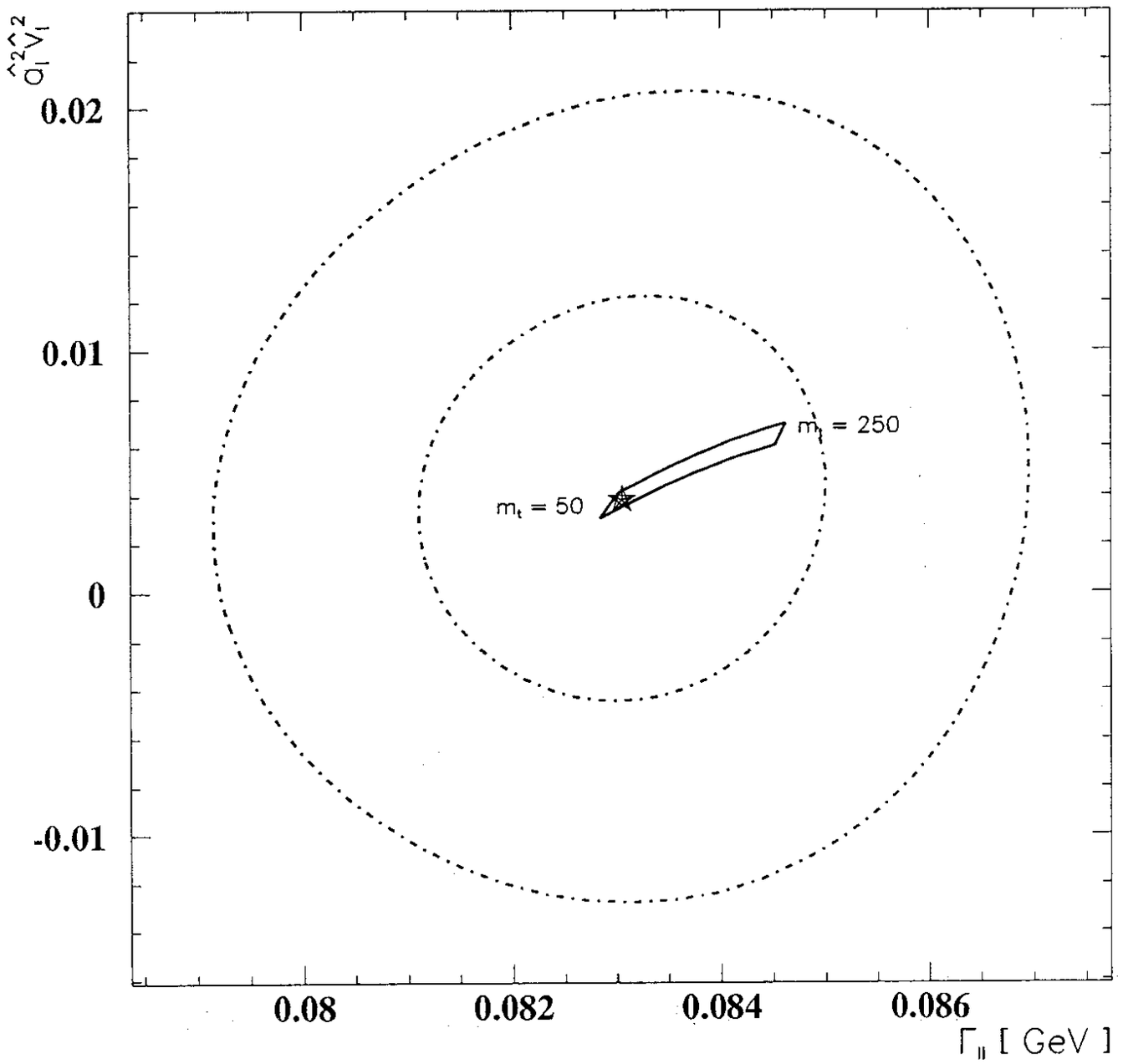
$\hat{a}_l^2 \hat{v}_l^2$
0.02
0.01
0
-0.01
$m_t$ = 250
$m_t$ = 50
0.08
0.082
0.084
0.086
$\Gamma_{ll}$ [ GeV ]

# Figure 4

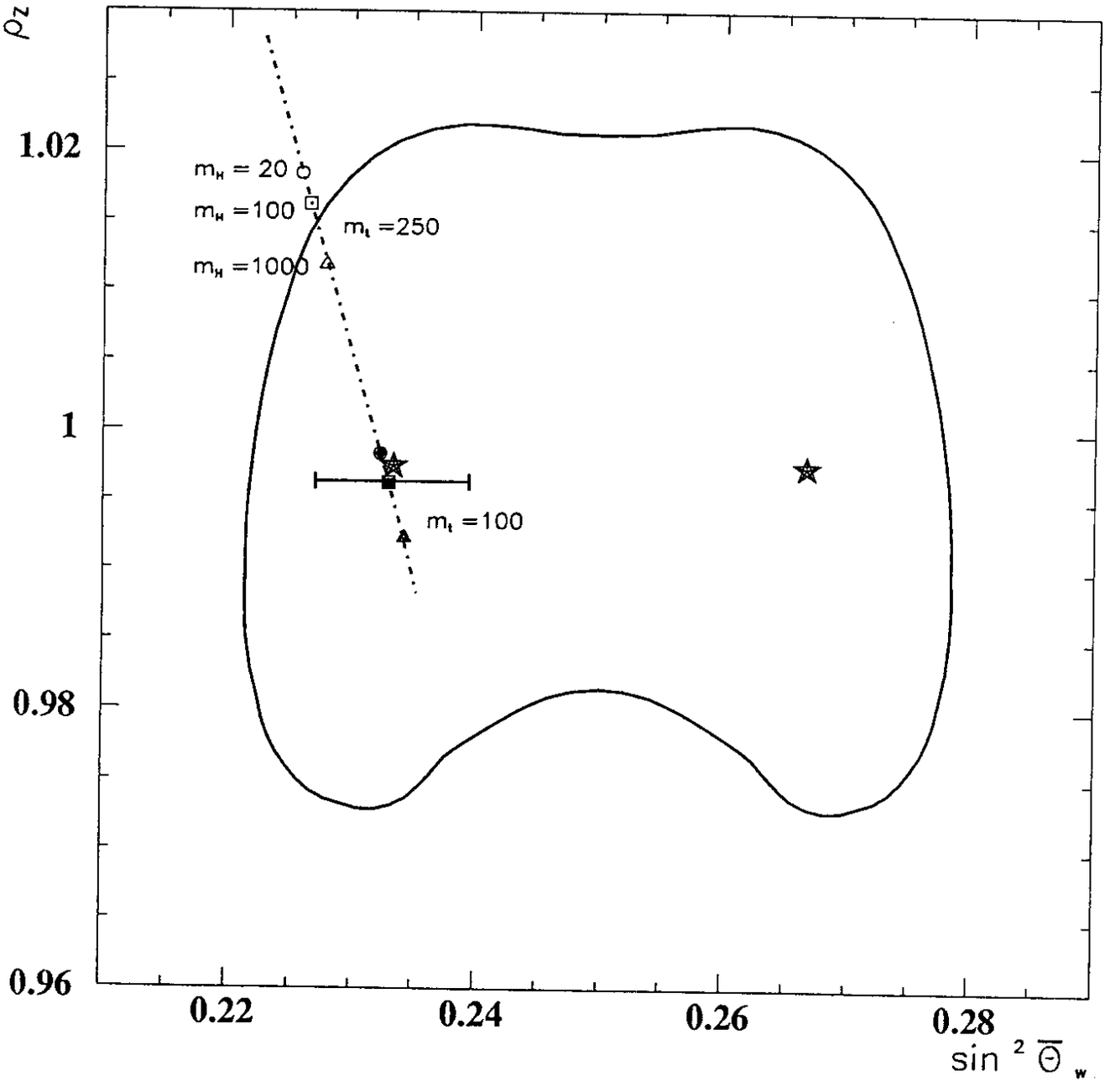


Imprimé au CERN. Prix : 0.80 Fr.